Formation of Ceramide/Sphingomyelin Gel Domains in the Presence of an Unsaturated Phospholipid: A Quantitative Multiprobe Approach

Bruno M. Castro,* Rodrigo F. M. de Almeida,*† Liana C. Silva,* Alexander Fedorov,* and Manuel Prieto*
*Centro de Química-Física Molecular, Instituto Superior Técnico, Lisbon, Portugal; and †Departamento de Química e Bioquímica, Faculdade de Ciências da Universidade de Lisboa, Lisbon, Portugal

ABSTRACT To better understand how ceramide modulates the biophysical properties of the membrane, the interactions between palmitoyl-ceramide (PCer) and palmitoyl-sphingomyelin (PSM) were studied in the presence of the fluid phospholipid palmitoyl-oleoyl-phosphatidylcholine (POPC) in membrane model systems. The use of two fluorescent membrane probes distinctly sensitive to lipid phases allowed a thorough biophysical characterization of the ternary system. In these mixtures, PCer recruits POPC and PSM in the fluid phase to form extremely ordered and compact gel domains. Gel domain formation by low PCer mol fraction (up to 12 mol %) is enhanced by physiological PSM levels (~20–30 mol % total lipid). For higher PSM content, a three-phase situation, consisting of fluid (POPC-rich)/gel (PSM-rich)/gel (PCer-rich) coexistence, is clearly shown. To determine the fraction of each phase a quantitative method was developed. This allowed establishing the complete ternary phase diagram, which helps to predict PCer-rich gel domain formation and explains its enhancement through PSM/PCer interactions.

INTRODUCTION

Sphingolipids (SL) are important plasma membrane lipids that play an essential role in membrane-mediated processes such as cell signaling, senescence, growth, and differentiation (1,2). It is well known that SL are able to laterally segregate from glycerophospholipids in the membrane. This leads to the formation of membrane domains, which are involved in the activation/inhibition of those biological processes (1,3). Although these lateral assemblies can arise solely due to lipid-lipid interactions, in cell membranes lipid-protein and protein-protein interactions also play an important role in the formation and function of these domains (4,5).

Over the past two decades, the discovery of SL signaling pathways has stimulated research on the biochemistry and biophysics of these molecules (reviewed in the literature (6,7)). Sphingosine, sphingosine-1-phosphate and especially ceramide (Cer) are examples of SL that have emerged as second messengers or metabolic signals (8–10). In resting cells, the level of Cer in the plasma membrane is very low. However, it can rise severalfolds after a wide variety of stress stimuli (11), reaching up to 10 mol % of total membrane lipid in cells undergoing apoptosis (12). Sphingomyelin (SM) hydrolysis by sphingomyelinase (SMase) is the main process responsible for increasing Cer plasma membrane levels, and it has been proposed that SL/Cholesterol (Chol)-enriched membrane domains are the primary site for action of this enzyme (13). The mechanisms by which Cer plays its biological roles are still unknown. It has been proposed that Cer formation would lead to alterations of membrane biophysical properties, e.g., inducing the formation of large platforms. These platforms would be responsible for the clustering of receptors and proteins, and for the initiation of signal transduction (reviewed in the literature (8,13)). However, recent studies have shown that the size of Cer-rich domains is highly dependent on the lipid composition of the membrane (14–17). A thorough characterization of Cer interactions with other membrane lipid species, namely SM, is required to understand how Cer modulates both membrane biophysical properties and biological processes.

Direct cause-effect relationships are often difficult to establish in membrane related phenomena, especially when biophysical changes are involved, as in the case of Cer. Hence, it is necessary to know the relation between the extent of membrane alterations induced by a particular lipid and the concentration of that lipid, in a system where the global lipid composition is controlled and known, as in the case of model membranes. This type of system is suitable for systematic studies that mimic the membrane biophysical alterations that take place after Cer formation in the plasma membrane. In model membranes, Cer is able to increase the molecular order of the bilayer and to induce the formation of gel domains (18–23). Additionally, these studies show that Cer-induced alterations are dependent on membrane lipid composition: i), in phosphatidylcholine (PC)/Cer and (SM)/Cer binary mixtures, Cer-rich and Cer-poor domains are formed (18,21,23, 24); ii), in more complex mixtures containing SM, Cer/SM gel domains are reported (14,19,22). Recently, we observed that physiological amounts of *N*-palmitoyl-ceramide (PCer) are able to induce the formation of a highly ordered PCer/*N*-palmitoyl-sphingomyelin (PSM) gel in 1-palmitoyl-2-oleoyl-*sn*-glycero-3-phosphocholine (POPC)/Chol/PSM mixtures (15), which was abolished with the increase of Chol content.

To better understand the formation of Cer/SM gel domains, the characterization of Cer/SM interactions in the presence of

Submitted February 26, 2007, and accepted for publication May 7, 2007.

Address reprint requests to Rodrigo F. M. de Almeida, CQFM, Instituto Superior Técnico, Av. Rovisco Pais, 1049-001 Lisboa, Portugal. Fax: 351-218-464-455; E-mail: r.almeida@mail.ist.utl.pt.

Editor: Akihiro Kusumi.

0006-3495/07/09/1639/12 $2.00

doi: 10.1529/biophysj.107.107714

a fluid phospholipid representative of the plasma membrane outer leaflet, such as POPC (25), is required. The phase behavior and properties of the binary systems POPC/PSM and POPC/PCer are well characterized (23,26). The representation of a phase diagram at fixed temperature in two-dimensions describing the relation between Cer levels and the phase behavior of the system is only possible for mixtures with up to three components. Thus, the system of choice for this study was POPC/PSM/PCer. The previous characterization of the probes' photophysical properties in POPC/PSM and POPC/PCer mixtures (23,26), allowed the use of a methodology in which the screening of all lipid mixtures with up to 12 mol % of PCer gave a complete description of the POPC/PSM/PCer ternary system.

MATERIALS AND METHODS

Materials

POPC, PSM, and PCer were obtained from Avanti Polar Lipids (Alabaster, AL). 1,6-diphenyl-1,3,5-hexatriene (DPH) and *trans*-parinaric acid (*t*-PnA) were from Molecular Probes (Leiden, The Netherlands). All organic solvents were UVASOL grade from Merck (Darmstadt, Germany).

Liposome preparation

Multilamellar vesicles (MLV) (total lipid concentration 0.1 mM) containing the adequate lipids and DPH were prepared by standard procedures (e.g., Mateo et al. (27)). The suspension medium was sodium phosphate 10 mM, NaCl 150 mM, EDTA 0.1 mM buffer (pH 7.4). The samples were reequilibrated by freeze-thaw cycles and incubation at $T > 90$°C. For studies with *t*-PnA, samples were slowly brought to room temperature and the probe was then added from an ethanol stock solution. The samples were reequilibrated again by freeze-thaw cycles and subsequently kept overnight at 4°C. Before the measurements, the samples were slowly brought to room temperature and maintained at this temperature at least for 1 h. The probe/lipid ratios used were 1:200 for DPH and 1:500 for *t*-PnA. The total SL mol fraction (X_{SL} = PSM mol fraction (X_{PSM}) + PCer mol fraction (X_{PCer})) was kept constant.

The concentration of POPC, PSM, and PCer stock solutions was determined gravimetrically with a high precision balance (Mettler Toledo UMT2). Probe concentration was determined spectrophotometrically using ε(DPH, 355 nm, chloroform) = 80.6×10^3 $M^{-1}cm^{-1}$ (28) and ε(*t*-PnA, 299.4 nm, ethanol) = 89×10^3 $M^{-1}cm^{-1}$ (29).

Absorption and fluorescence measurements

All measurements were performed in 0.5 cm × 0.5 cm quartz cuvettes and under magnetic stirring. The absorption and steady-state instrumentation was previously described (30). Fluorescence steady-state measurements were carried out in a SLM-Aminco 8110 Series 2 spectrofluorometer. The steady-state fluorescence anisotropy, $\langle r \rangle$, was calculated through the expression (e.g., Lakowicz (31))

$$\langle r \rangle = (I_{VV} - G \times I_{VH})/(I_{VV} + 2 \times G \times I_{VH}), \quad (1)$$

in which the different intensities (blank subtracted) are the steady-state vertical and horizontal components of the fluorescence emission with excitation vertical (I_{VV} and I_{VH}, respectively) and horizontal (I_{HV} and I_{HH}, respectively) to the emission axis. The latter pair of components is used to calculate the *G* factor ($G = I_{HV}/I_{HH}$). The excitation (λ_{exc}) / emission (λ_{em}) wavelengths were 358 / 430 nm for DPH and 303 / 405 nm for *t*-PnA. The temperature (24°C) (±0.2°C within replicates) was maintained by a Julabo F25 circulating water bath and controlled with 0.1°C precision directly inside the cuvette with a type-K thermocouple (Electrical Electronic, Taipei, Taiwan).

The fluorescence decay measurements were obtained by the single photon-timing technique with laser pulse excitation (e.g., Birch and Imhof (32)). Measurements with *t*-PnA ($\lambda_{exc} = 295$ nm and $\lambda_{em} = 405$ nm) were performed using a secondary laser of Rhodamine 6G (26). For DPH measurements ($\lambda_{exc} = 360$ nm and $\lambda_{em} = 430$ nm) a Ti-Sapphire laser (33) was used. The fitting curves to the experimental decays were obtained by a nonlinear least squares iterative reconvolution method based on the Marquardt algorithm (e.g., Birch and Imhof (32)). For a fluorescence decay described by a sum of exponentials, where α_i is the normalized preexponential (or amplitude) and τ_i is the lifetime of the decay component *i*, the lifetime-weighted quantum yield and the mean fluorescence lifetime are respectively given by:

$$\bar{\tau} = \sum_i \alpha_i \tau_i, \quad (2)$$

and

$$\langle \tau \rangle = \sum_i \alpha_i \tau_i^2 / \sum_i \alpha_i \tau_i. \quad (3)$$

Determination of *t*-PnA phase behavior and gel phase fraction in POPC/PSM/PCer mixtures

The partition coefficient of *t*-PnA between gel and fluid phases, $K_p^{g/f}$, in POPC/PSM binary mixtures was determined from the variation of the photophysical parameters of this probe with the mol fraction of the fluid (*f*), X_f, and the gel phase (*g*), X_g, respectively. The composition of the mixtures and the mol fraction of each phase (X_i) were taken from the tie-line at 24°C of the respective phase diagram (26). The partition coefficient is an equilibrium constant that quantifies the partition of the probe between the two distinct phases present in these binary mixtures (*f* and *g*), and consequently is independent of the particular composition of the mixtures.

The partition coefficient is calculated according to the following expressions (15/26): i), from mean fluorescence lifetime, $\langle \tau \rangle$,

$$\langle \tau \rangle = \frac{\langle \tau \rangle_g K_p X_g + \bar{\tau}_f/\bar{\tau}_g \langle \tau \rangle_f X_f}{K_p X_g + \bar{\tau}_f/\bar{\tau}_g X_f}, \quad (4)$$

and ii), from steady-state fluorescence anisotropy with the absence of significant spectral shifts, $\langle r \rangle$,

$$\langle r \rangle = \frac{\langle r \rangle_g K_p X_g + \bar{\tau}_f/\bar{\tau}_g \langle r \rangle_f X_f}{K_p X_g + \bar{\tau}_f/\bar{\tau}_g X_f}, \quad (5)$$

where X_i is the phase mol fraction, $\langle \tau \rangle_i$, $\bar{\tau}_i$, and $\langle r \rangle_i$ are the mean fluorescence lifetime, the lifetime-weighted quantum yield, and steady-state fluorescence anisotropy of the probe in phase *i*, respectively. K_p is obtained by fitting the equations to the data as a function of X_i. Conversely, these equations can be used to determine X_i in a given sample if the K_p and the parameter in question for the pure coexisting phases are known. The molar absorption coeffcient of the probes is considered phase independent.

RESULTS

t-PnA prefers the PSM-rich gel phase in POPC/PSM gel/fluid mixtures

To investigate the changes induced by PCer in the binary system POPC/PSM two fluorescent membrane probes were used, DPH and *t*-PnA. To retrieve information from the

comparison of the photophysical parameters of these probes, it is necessary to know how they distribute between the different phases present. In previous studies it was shown that: i), in the binary mixture POPC/PSM, DPH presents an approximately equal partition between gel and fluid phases ($K_p^{g/f} \sim 1$) (26), and ii), this probe is excluded from the PCer-enriched gel domains, whereas iii), *t*-PnA presents a high preference for PCer-rich gel phase ($K_p^{g/f} \sim 4.5$) (23) in relation to the fluid POPC-rich phase. The $K_p^{g/f}$ of *t*-PnA in POPC/PSM mixtures was determined from the steady-state fluorescence anisotropy variation (Eq. 5; Fig. 1). The composition of each phase was taken from the tie-line at 24°C of the POPC/PSM phase diagram (26). The $K_p^{g/f}$ obtained (1.88 ± 0.14) shows that in these binary mixtures *t*-PnA has a preferential partition (thought not strong) toward the PSM-rich gel phase, again, a behavior clearly distinct from that of DPH.

PCer changes the gel-fluid coexistence region in POPC/PSM mixtures

The fluorescence anisotropy of a probe gives information about the rotational speed and freedom of the fluorophore, reflecting the rigidity of its environment. For the probes *t*-PnA and DPH, the fluorophores are located in the hydrophobic region of the bilayer, being thus reporters of the lipid acyl chains. In addition, by combining the fluorescence anisotropy of the two probes with the knowledge of their lipid phase behavior, it is possible to detect and quantify the fraction of membrane regions that present distinct biophysical properties. The variation of the steady-state fluorescence anisotropy of *t*-PnA and DPH as a function of sphingolipid mol fraction ($X_{SL} = X_{PSM} + X_{PCer}$) for different POPC/PSM/PCer mixtures is represented in Fig. 2. In the absence of PCer (*open circles*), the anisotropy of both probes undergoes a sharp increase with the X_{PSM}, reflecting the formation of the PSM-rich gel phase (26). DPH anisotropy increases linearly with PSM content (Fig. 2 *B*), reflecting the probe's $K_p^{g/f} \sim 1$ and similar quantum yield in the gel and fluid phases (26). By contrast, *t*-PnA anisotropy has a more pronounced increase due to its higher partition to—and quantum yield in—the PSM-rich gel phase. In the presence of PCer, *t*-PnA anisotropy values increase relatively to the POPC/PSM binary mixtures. This effect is higher for the low X_{SL} regime. Accordingly, the increase in the anisotropy values with X_{SL} is successively attenuated with the increase in the mol fraction of PCer. This result shows that PCer is ordering the lipid bilayer, probably through the formation of a PCer-rich gel phase (23). Note that for mixtures where only gel phase is

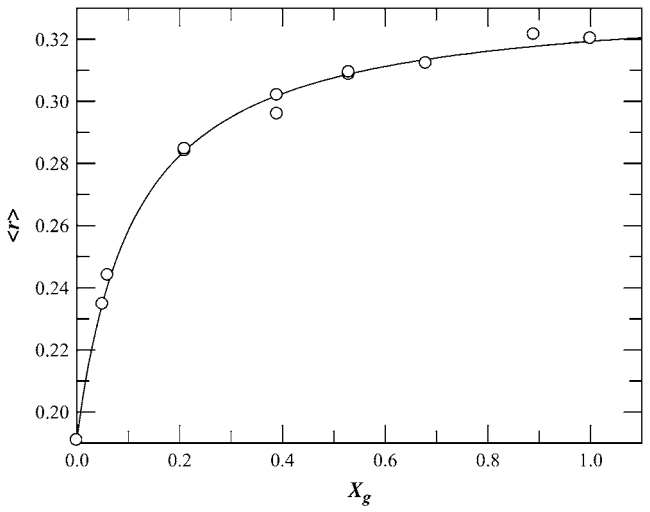

FIGURE 1 Determination of *t*-PnA partition coefficient (K_p) between PSM-rich gel and POPC-rich fluid phase in POPC/PSM binary mixtures. The steady-state fluorescence anisotropy of *t*-PnA is represented as a function of the gel phase fraction in POPC/PSM mixtures. The gel phase mol fraction (X_g) was taken from the tie-line at 24°C of the POPC/PSM binary phase diagram (26). The line represents the nonlinear fit of Eq. 5 to the experimental data with $K_p^{g/f} = 1.88 \pm 0.14$.

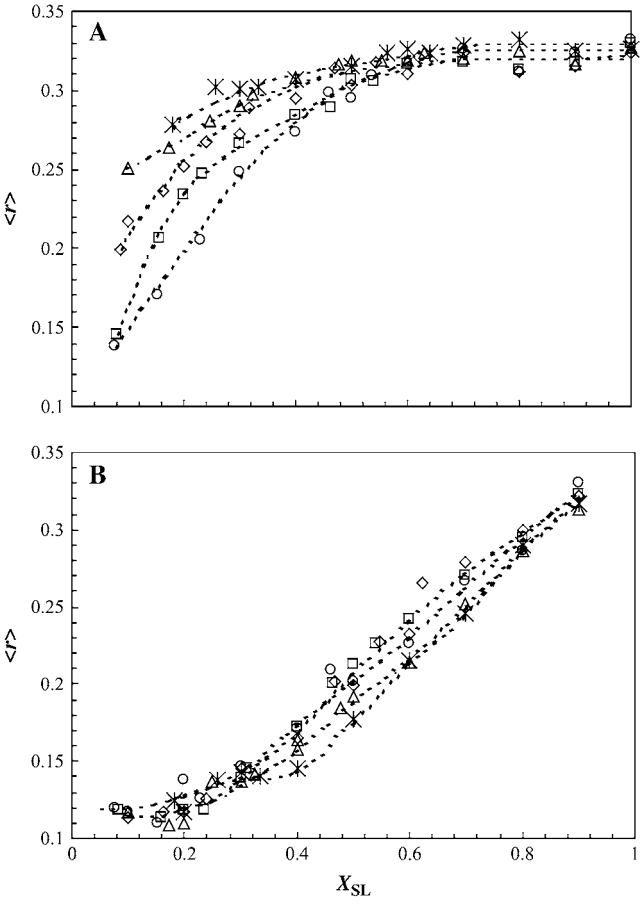

FIGURE 2 Effect of PCer in POPC/PSM mixtures. (*A*) *t*-PnA and (*B*) DPH steady-state fluorescence anisotropy as a function of total sphingolipids mol fraction ($X_{SL} = X_{PSM} + X_{PCer}$), in POPC/PSM mixtures containing 0 (○), 2 (□), 4 (◇), 8 (△), and 12 (*) mol % PCer. The dashed lines are merely a guide to the eye. The error bars are within the size of the symbol and correspond to at least three independent samples.

present ($X_{PSM} > 0.70$), the exchange of PSM by PCer does not affect *t*-PnA anisotropy. Conversely, DPH anisotropy changes are much less notable (Fig. 2 *B*). However, for high X_{PCer}, DPH anisotropy values indeed present a small but yet significant decrease, as shown in Fig. 3 (with data collected from Fig. 2 *B*). This result suggests that PCer is inducing the formation of an extremely ordered gel phase that is able to exclude DPH, as previously shown for other lipid mixtures containing PCer (15,23).

t-PnA time-resolved fluorescence reports the formation of PCer-rich gel domains

The fluorescence intensity decay of *t*-PnA in the POPC/PSM/PCer system was obtained. The mean fluorescence lifetime (calculated from Eq. 3) is represented in Fig. 4. The variations observed are consequence of alterations of the nonradiative rate constant, giving complementary information to the fluorescence anisotropy. In the case of studies in lipid bilayers, the presence of a long fluorescence lifetime component is a fingerprint for gel phase (27,29,30), and allows the distinction between two different situations where the order of the lipid bilayer is similarly increased: i), less disordered bulk fluid phase; ii), the presence of small amounts of gel phase. In addition, time-resolved measurements should always be performed in this type of studies, because according to the Perrin equation a decrease in the probe's fluorescence lifetime could lead to an increase in its steady-state fluorescence anisotropy (see, e.g., Lakowicz (31)). *t*-PnA mean fluorescence lifetime (Fig. 4) presents a behavior similar to the one observed for its fluorescence anisotropy (Fig. 2 *A*). In the absence of PCer there is a sharp increase with X_{SL}, which is successively attenuated for higher X_{PCer}. It should be emphasized that the longer mean fluorescence lifetime values are typical of a gel phase (29), reporting the compact environment surrounding the fluorophore. This result is similar to the one obtained for *t*-PnA in POPC/PCer mixtures (23). *t*-PnA mean fluorescence lifetime was shown to be extremely sensitive to the PCer-rich gel phase due to the presence of a long lifetime component (>30 ns) in its fluorescence decay (23). Analogously, the high fluorescence anisotropy and mean fluorescence lifetime values for *t*-PnA obtained in POPC/PSM/PCer mixtures constitute strong evidence for the formation of a PCer-rich gel phase. It further shows that the gel domains are exceptionally ordered, because the increase in anisotropy is due to an increase of the rotational correlation time and hindered rotation, compensating for the raise of fluorescence lifetime of the probe (23,31). The long lifetime component of *t*-PnA fluorescence decay is always high (>30 ns) (Fig. 5), clearly showing that a gel phase is present in all mixtures studied. According to the binary phase diagram POPC/

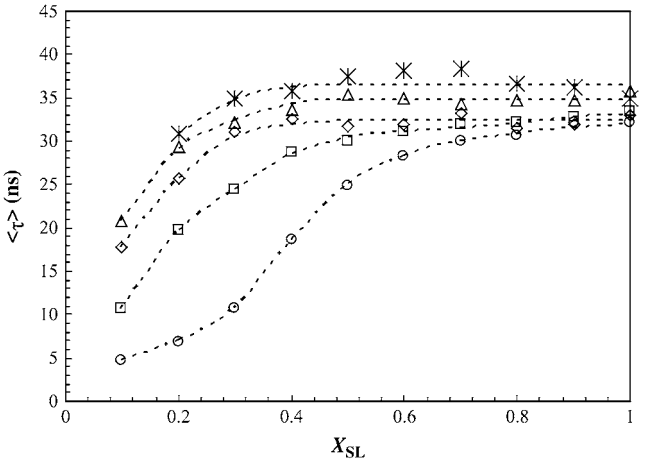

FIGURE 4 Effect of PCer on *t*-PnA's mean fluorescence lifetime ($\langle\tau\rangle$) in POPC/PSM mixtures containing 0 (○), 2 (□), 4 (◇), 8 (△), and 12 (*) mol % PCer, as a function of total sphingolipids mol fraction ($X_{SL} = X_{PSM} + X_{PCer}$). The dashed lines are merely a guide to the eye.

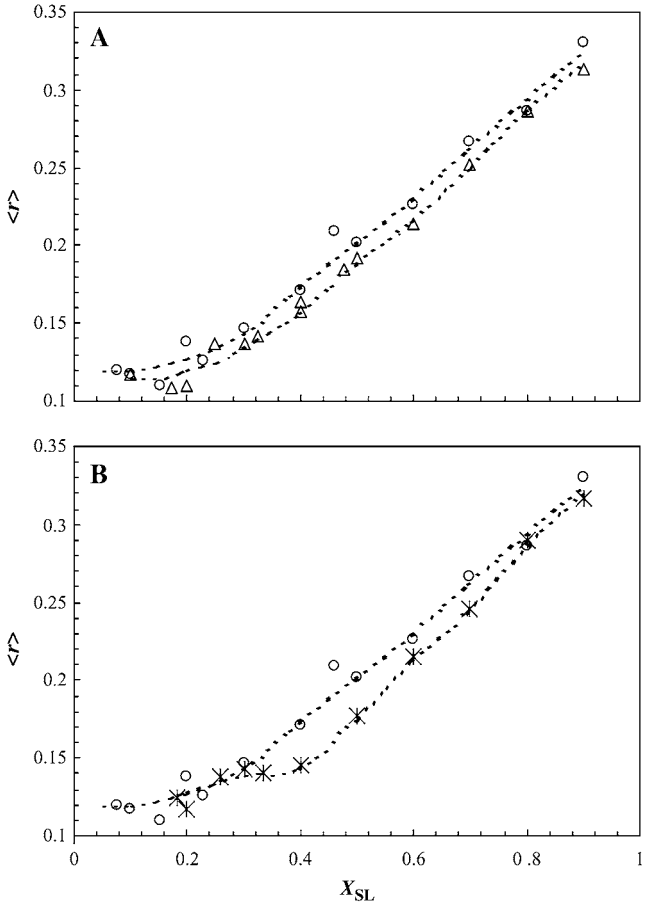

FIGURE 3 Formation of a gel phase that excludes DPH: effect of PCer on DPH steady-state fluorescence anisotropy in POPC/PSM mixtures containing (*A*) 0 (○) and 8 (△) mol % PCer, and (*B*) 0 (○) and 12 (*) mol % PCer as a function of total sphingolipids molar fraction ($X_{SL} = X_{PSM} + X_{PCer}$). The data present were taken from Fig. 2 *B*. The dashed lines are merely a guide to the eye. The error bars are within the size of the symbol and correspond to at least three independent samples.

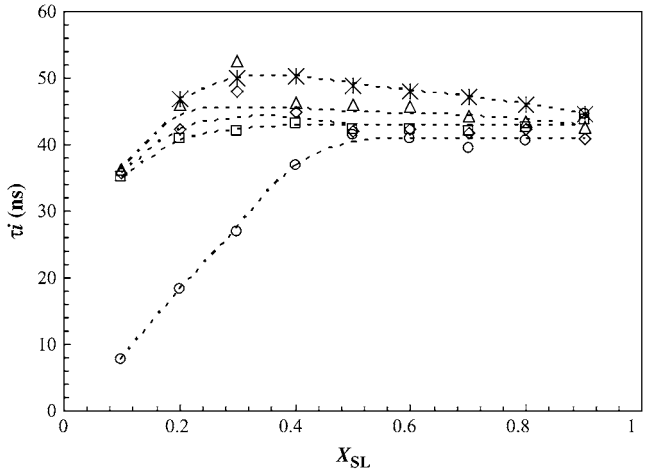

FIGURE 5 Fluorescence lifetime of the long component of *t*-PnA fluorescence decay, in POPC/PSM mixtures containing 0 (○), 2 (□), 4 (◇), 8 (△), and 12 (*) mol % PCer, as a function of total sphingolipids mol fraction ($X_{SL} = X_{PSM} + X_{PCer}$). The dashed lines are merely a guide to the eye.

PCer (23), 4 mol % PCer is the minimal fraction required to induce gel-fluid phase coexistence at 24°C. On the other hand, in more complex mixtures containing SM, Cer is able to associate with SM to form gel domains (14,15). Therefore, without additional calculations it is not possible to conclude about the composition of the gel domains (see Discussion).

Unlike *t*-PnA, DPH fluorescence lifetime increases slightly with X_{SL} and is almost invariant in the presence of PCer (data not shown). DPH has a similar quantum yield in gel and fluid phases, and the mean fluorescence lifetime of this probe does not present pronounced dependence on the lipid phase (28).

DISCUSSION

DPH and *t*-PnA provide complementary information

In this work two probes that present different phase partitioning behavior were used, DPH and *t*-PnA. In general, it is considered that DPH distributes indistinctly between gel and fluid phases ($K_p^{g/f} \sim 1$) (35) (as in the case of POPC/PSM binary mixtures (26)). However, in PCer containing mixtures this probe is excluded from the PCer-rich gel phase, reporting the biophysical properties of PCer-poor phases (15,23). On the other hand, *t*-PnA presents a high preference for PCer-rich gel phase ($K_p^{g/f} \sim 4.5$) (23), and therefore is an exceptional reporter of this gel phase. Consequently, by combining these two membrane probes complementary information is obtained. In addition, the quantum yield of the probes behaves differently, i.e., whereas the DPH quantum yield is weakly sensitive to the lipid phase, *t*-PnA presents quantum yield values and fluorescence lifetime components that are typical of each phase. The fact that for both probes the fluorescence anisotropy is high in the gel and low in the fluid, together with the previously mentioned differences, allows for a detailed characterization of the lipid phases that are formed in the ternary system under investigation. In this study, the gel-fluid partition coefficient of *t*-PnA was determined for POPC/PSM binary mixtures (Fig. 1). It has been described that in mixtures presenting gel-fluid coexistence, *t*-PnA has a preferential partition toward the gel phase (29). Indeed, a $K_p^{g/f} > 1$, as determined here, is in accordance with that description. This equilibrium constant allows for the determination of *t*-PnA gel-gel partition coefficient ($K_p^{g/g}$) in PSM/PCer mixtures, which is given by the ratio of the gel-fluid partition coefficient of this probe in POPC/PCer (~4.5) (23) and in POPC/PSM binary mixtures (~1.88). The value obtained ($K_p^{g/g} = 2.4$) shows that in mixtures presenting PSM-rich and PCer-rich gel-gel separation, *t*-PnA will preferentially report the biophysical properties of the gel phase rich in PCer. In this very specific case, a stepwise methodology (15,23) proved to be quite complex. The PSM/PCer binary system presents several experimental difficulties. These are due, in part, to the fact that gel/gel phase separation occurs in this system. For example, both *t*-PnA and DPH photophysical parameters present only slight variations in PSM/PCer mixtures. Therefore, the phase partitioning behavior of the probes in this binary system is difficult to determine. On the other hand, *t*-PnA gel-fluid partition coefficient in POPC/PSM and POPC/PCer (23) mixtures allowed the determination of the phase partition of this probe in PSM/PCer binary mixtures. This calculation is essential for the characterization of PCer/PSM interactions, helping to understand the nature of the gel phase induced by PCer that is formed in the ternary mixtures of this work. Additionally, this equilibrium constant will be required for the resolution of the PSM/PCer binary phase diagram (currently being investigated).

Quantifying PCer/PSM association in the presence of POPC

In this work, *t*-PnA fluorescence lifetime values (Figs. 4 and 5) show that 2 mol % PCer is enough to induce gel phase formation in fluid POPC/PSM mixtures ($X_{PSM} < 0.28$ (26)). The same mol fraction of PCer in POPC mixtures has only an ordering effect on the fluid membrane, but does not induce the formation of a gel phase (23). Thus, it is concluded that in POPC/PSM/PCer mixtures the ability of PCer to form gel domains is enhanced by PSM, probably forming a PCer/PSM-rich gel phase in a similar way as in POPC/Chol/PSM/PCer mixtures (15). In this study, we have calculated the gel fraction formed by PCer in POPC/PSM mixtures for which only a fluid phase would be present (Table 1). This was carried through Eq. 4, using the variation of *t*-PnA mean fluorescence lifetime (Fig. 4), and its photophysical parameters in pure gel and fluid phases taken from Silva et al. (23).

Although in mixtures containing 10 mol % SL, gel-fluid phase coexistence occurs for lower amounts of PCer than for

TABLE 1 Gel phase mol fraction (X_g) formed in POPC/PSM/PCer mixtures (total sphingolipid mol fraction, $X_{SL} = X_{PSM} + X_{PCer}$)

	X_{PCer}				
X_{SL}	0	0.02	0.04	0.08	0.12
X_{PCer}	*	*	*	0.05	0.10
0.10	*	0.01	0.03	0.05	†
0.20	*	0.04 (0.55)	0.09 (0.54)	0.12 (0.35)	0.15 (0.19)

The gel fraction was calculated from *t*-PnA mean fluorescence lifetime (Eq. 2–4) and the photophysical parameters in pure gel and fluid phases were taken from (23). The values in brackets are indicative calculations of the mol fraction of PSM in the PCer-rich gel phase, assuming that no POPC is present in this phase. For comparison, the values of X_g obtained in binary POPC/PCer mixtures at 24°C (23) are presented in the first row.

*No gel phase occurs for these mixtures (23,26).

†For this X_{PCer} only mixtures containing $X_{SL} > 0.12$ are possible.

the binary system POPC/PCer, where gel-fluid coexistence starts with 4 mol % PCer (23), the X_g values are similar in both systems. This result clearly shows that the solubility of PCer in the POPC/PSM fluid is lower than in the POPC fluid, even though PCer/PSM association in the gel phase is not happening. In mixtures containing 20 mol % SL, the gel fraction is higher than the mol fraction of PCer present in the mixtures. Thus, to respect conservation of the total gel fraction (mass balance), PSM molecules must exist in this gel phase. As a consequence, the gel domains induced by PCer in these mixtures result from the association of this lipid with the PSM previously in the fluid phase. Note that PCer/PSM gel domains formation is observed for physiological levels of PSM (~20–30% of total lipid of the external leaflet of plasma membrane (36)), indicating that this association may occur in biological membranes.

For the mixtures where PCer/PSM gel domains are formed ($X_{SL} = 0.2$), a first estimation of the composition of the PCer-rich gel phase (Table 1) was determined from the gel fractions previously calculated, assuming that all PCer and no POPC is participating in the formation of this phase. For low amounts of PCer (2 and 4 mol %) ~50% of the PCer-rich gel phase is composed of PSM, whereas for higher amounts of PCer, the PSM fraction present in this phase becomes successively smaller. This result is in accordance with a previous study of POPC/PSM/PCer mixtures, where the authors observed that PCer-enriched microdomains formation was higher in these ternary mixtures than in POPC/PCer binary mixtures, due to a preferential interaction of PSM with PCer (19). Although previous studies have shown that in SM/Cer binary system there is immiscibility of the two lipid species in the gel phase (22,24), in the case of more complex mixtures, there is evidence suggesting the association of these lipids (14,15,19,22).

Another evidence for PCer/PSM gel phase formation comes from DPH fluorescence anisotropy values. Fig. 3 shows that DPH anisotropy values are lower in mixtures containing PCer than in POPC/PSM mixtures. Studies carried out in different Cer-containing lipid mixtures have shown that DPH is excluded from the Cer-rich (gel) phase (15,23,37), which apparently is a characteristic of this phase. In this work, the substitution of PSM by PCer lowers the gel phase fraction that DPH is able to report (i.e., POPC/PSM gel). Thus, in POPC/PSM/PCer mixtures where PCer- and/or PCer/PSM-rich gel phase is formed, DPH presents lower fluorescence anisotropy values than in POPC/PSM binary mixtures.

To confirm that DPH is excluded from the PCer/PSM gel domains, the predicted anisotropy values of DPH for the gel fractions previously obtained (Table 1) were calculated, assuming that DPH distribution is equal between gel and fluid phases ($K_p^{g/f} = 1$) (38) and using Eq. 5. The values are given in Table 2 (the following DPH photophysical parameters were used: $\langle r \rangle_g = 0.34$, $\langle r \rangle_f = 0.13$, $\bar{\tau}_g = 8$ns, $\bar{\tau}_f = 6$ns (15)). The predicted values are systematically higher than the experimental ones, showing quantitatively the formation of a gel phase that is able to exclude DPH. Once that DPH is able to report the PSM-rich gel phase in POPC/PSM binary mixtures (26), the gel phase formed in POPC/PSM/PCer ternary mixtures must be extremely ordered and compact. This is in agreement with *t*-PnA fluorescence lifetime and anisotropy high values. The exclusion of DPH is in accordance with a

TABLE 2 DPH exclusion from the PCer-rich gel phase: experimental and predicted DPH steady-state fluorescence anisotropy in POPC/PSM/PCer mixtures containing 0.10 and 0.20 as total mol fraction of sphingolipid ($X_{SL} = X_{PSM} + X_{PCer}$) (Table 1)

	X_{PCer}				
X_{SL}	0.02	0.04	0.08	0.12	
0.10	0.119 ± 0.002	0.113 ± 0.004	0.12 ± 0.01	*	$\langle r \rangle_{experimental}$
	0.13	0.14	0.14	*	$\langle r \rangle_{predicted}$
0.20	0.119 ± 0.003	0.118 ± 0.009	0.11 ± 0.01	0.117 ± 0.004	$\langle r \rangle_{experimental}$
	0.14	0.15	0.16	0.17	$\langle r \rangle_{predicted}$

The predicted values were calculated from Eq. 5. The PCer-rich gel phase fraction formed in these mixtures was obtained from *t*-PnA mean fluorescence lifetime (Table 1). For the calculations it was assumed that DPH had an equal partition between gel and fluid phases ($K_p^{g/f} \sim 1$) (38), and the probe's photophysical parameters in pure gel and fluid phases were taken from Silva et al. (23). The error of the experimental DPH anisotropy values is the standard deviation of at least three independent samples.

*For this X_{PCer} only mixtures containing $X_{SL} > 0.12$ are possible.

previous study, which reports that PCer associates with PSM forming a very tightly packed gel that excludes a pyrene-labeled Cer analog (19). Note that the increase in DPH anisotropy values with X_{PSM} is only reporting the formation of a PSM-rich gel phase from a POPC-rich fluid phase (26).

It seems that the enhancement of the Cer-rich (gel) domains is specific for SM, arising due to a stable hydrogen bonding network and van der Waals interactions between these SL (8,19). In model membranes containing Cer and 1,2-dipalmitoyl-*sn*-glycerol-3-phosphocholine, which is the glycerophospholipid corresponding to PSM (both present the same acyl chain and gel-fluid melting temperature (39,40)), the extent of Cer-rich (gel) phase formed in these mixtures is lower than in mixtures containing SM (19,22). These results rule out the possibility that Cer-rich domains enhancement results solely from the association of Cer with high temperature melting lipid, showing that SM/Cer interactions play a critical role in the formation of the Cer-rich gel phase.

Quantifying three lipid phases in coexistence

The combined use of *t*-PnA and DPH allowed the study of a complex three-phase situation, where a PCer/PSM gel, a PSM-rich gel, and a POPC-rich fluid phase coexistence was present. To our knowledge, few studies have shown three-phase coexistence in membranes containing Cer (14–16). This is not only related to inherent difficulties in studies with Cer, namely hydration problems (e.g., (21,24,41)), but because the coexistence of three lipid phases is extremely difficult to establish experimentally.

For the three-phase coexistence situation, the strategy employed to determine the gel fraction induced by PCer (Table 1) could not be used, because two distinct gel phases are present. Therefore, a novel approach was developed, which is based on the fluorescence parameters and partition coefficients of both probes between the three pairwise combination of the phases present. This methodology allowed the quantification of the mol fraction of each phase present in the ternary mixtures under study (Appendix I). The results obtained are summarized in Table 3.

In these mixtures, two distinct regimes are apparent: the low, and the high X_{PCer}. In the low X_{PCer} (2 and 4 mol %) regime, gel phase formation induced by PCer is enhanced for low X_{SL} (0.3 and 0.4). For higher SL amounts, the total gel phase fraction is similar to the one that is formed in the POPC/PSM binary system. Nonetheless, in mixtures containing PCer, the PSM-rich gel phase is slightly lower than in POPC/PSM mixtures, emphasizing PCer ability to recruit PSM molecules. Increasing X_{PCer}, PCer-rich gel phase enhancement by PSM increases successively, until 50 mol % SL with 8 mol % PCer are reached. For the mixtures containing 12 mol % PCer, it was only possible to accurately calculate the phase mol fractions for mixtures containing 30 and 40 mol % SL. This happened because the method is based on the variation of *t*-PnA photophysical parameters and phase behavior for the ternary mixtures (Appendix I). *t*-PnA presents an unfavorable partition coefficient for the fluid as well as a smaller quantum yield in this phase. Therefore, in a situation where the fluid phase fraction is low and PCer-rich gel phase fraction is high, *t*-PnA will present fluorescence properties indistinguishable between a system in the gel phase, and a system containing 10% or less of fluid phase. This is the case for the mixtures containing 12 mol % PCer and high X_{SL} (>0.40).

For mixtures containing 30 mol % SL with 8 or 12 mol % PCer, and 40 mol % SL with 12 mol % PCer, the PSM-rich gel phase is negligible and the PSM fraction in PCer-rich gel phase is high. These results show the remarkable PCer ability to recruit PSM molecules to induce the formation of a gel phase in model membranes, as recently observed in analogous systems containing Chol (14–16). Overall, these studies suggest that in cellular membrane where SM levels are high (1,26), Cer/SM gel domains may occur.

TABLE 3 Mol fraction of PSM-rich and PCer-rich gel phases (X_g^{PSM} and X_g^{PCer}, respectively) in POPC/PSM/PCer ternary mixtures

	X_{PCer}								
	0	0.02		0.04		0.08		0.12	
X_{SL}	X_g^{PSM}	X_g^{PSM}	X_g^{PCer}	X_g^{PSM}	X_g^{PCer}	X_g^{PSM}	X_g^{PCer}	X_g^{PSM}	X_g^{PCer}
0.30	0.05*	0.05	0.04	0.04	0.12	0	0.14	0	0.25
0.40	0.26*	0.24	0.06	0.23	0.13	0.12	0.18	0	0.34
0.50	0.47*	0.44	0.06	0.44	0.06	0.28	0.30	†	†
0.60	0.68*	0.65	0.05	0.66	0.03	0.42	0.25	†	†
0.70	0.89*	0.84	0.06	0.84	0.06	0.66	0.18	†	†

The total SL mol fraction ($X_{SL} = X_{PSM} + X_{PCer}$) that was spanned corresponds to the gel-fluid coexistence range of the POPC/PSM binary system at 24°C, i.e., $0.28 \leq X_{SL} \leq 0.75$, without the Mabrey and Sturtevant correction (26). The gel phase mol fractions were obtained from *t*-PnA mean fluorescence lifetimes (Fig. 4), using the equations described in Appendix I.

*Values taken from the tie-line at 24°C of the POPC/PSM binary phase diagram (26).

†For these mixtures the fluid phase fraction is always low. In this situation, *t*-PnA fluorescence properties, in which the quantitative method developed is based, are indistinguishable from those in a system entirely in the gel phase, because the probe presents an unfavorable partition coefficient and a small quantum yield in the fluid phase.

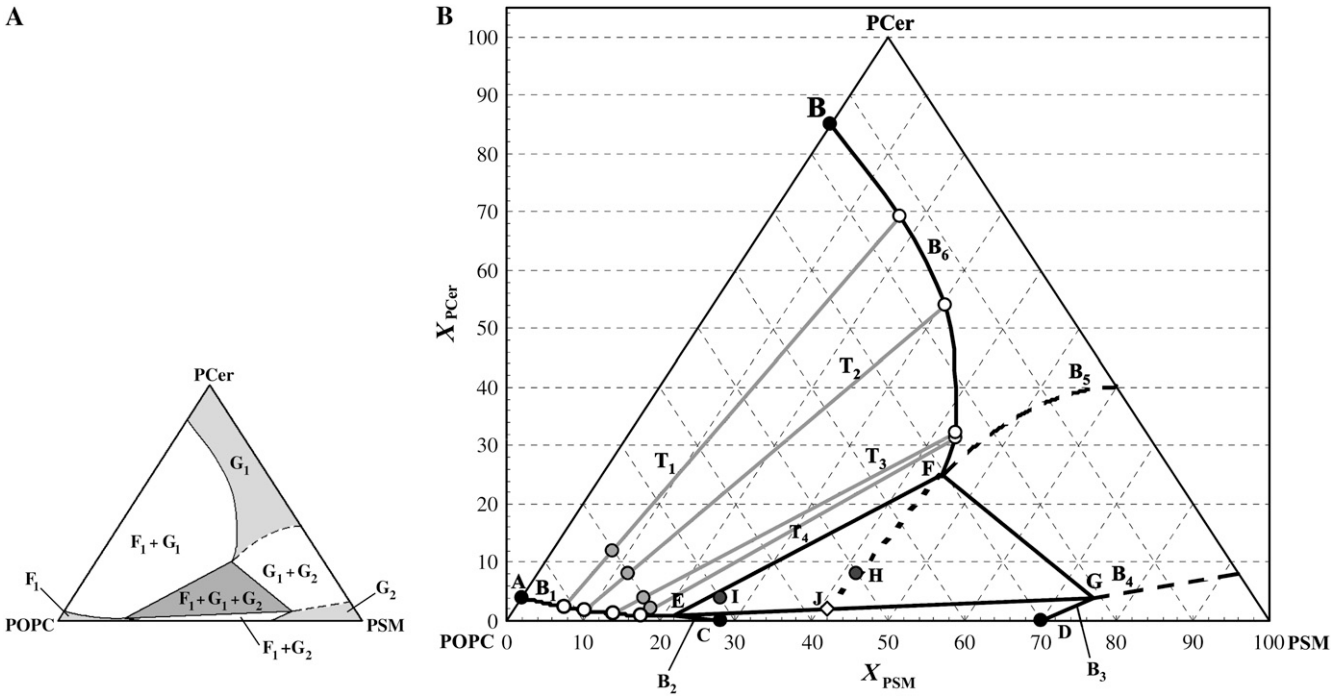

FIGURE 6 POPC/PSM/PCer ternary phase diagram at 24°C determined from the photophysical and phase-related properties of the two complementary fluorescent membrane probes *t*-PnA and DPH, together with quantification methodologies and an iterative procedure. (*A*) Ternary phase diagram highlighting the seven distinct regions identified. The abbreviations correspond to: F_1, POPC-rich fluid phase; G_1, PCer-rich gel, and G_2, PSM-rich gel phase. The colors correspond to the number of phases present in each region: light gray, one phase; white, two phases; dark gray, three phases. (*B*) Scaled POPC/PSM/PCer phase diagram. The lines B_1–B_6 represent the phase boundaries between one-phase and two-phase regions. Each side of the tie-triangle is a phase boundary that separates a two-phase region from a three-phase region. T_1–T_4 are the tie-lines for the $F_1 + G_1$ region that contain the ternary mixtures composed of $X_{SL} = 0.2$ and 2, 4, 8, and 12 mol % PCer (*solid light gray circles*), respectively. The open circles over B_1 and B_6 are the edges of the tie-lines. The direction and length of these tie-lines, together with points B and F allowed for the determination of B_6 (see text for further details). The points A, B and C, D are experimental points taken from the POPC/PCer (23) and the POPC/PSM (26) phase diagrams, respectively. H and I are illustrative for which three-phase coexistence was quantified (Table 3). The lever rule was exemplified for these points (Appendix II). J and the dashed line FJ are presented for a better exemplification of the lever rule. The full lines were experimentally determined. All the lines have strong experimental basis and are thermodynamically consistent. However, due to technical limitations discussed in the text, B_4 and B_5 are still under definition, being represented by dashed lines. These boundaries are the best estimations based on our own experimental data, thermodynamic principles (42), and calorimetric studies (24). All the remainder of the phase diagram was determined independently of the exact position of B_4 and B_5.

POPC/PSM/PCer ternary phase diagram

The quantitative method based on the complementary information retrieved from each fluorescent probe allowed the determination of the POPC/PSM/PCer ternary phase diagram at 24°C (Fig. 6). The phase diagram was obtained by an iterative method. In this method, different configurations for a phase diagram of the type of Fig. 6 *A* were assayed, and the phase fractions and compositions computed. These were compared with the experimental values (Tables 1 and 3). Then, configurations with minimal deviations between the two sets of values were selected, and configurations close to those ones were tried, and so on and so forth, until no further improvement in matching the experimental values to the values calculated from the diagram was obtained. Best trial in an iteration was the one for which the maximal difference between an experimental and a calculated value was smaller, and also for which the deviations were more randomized, i.e., the points for which a certain phase and/or component were given in excess were compensated by those for which those values were given in default. The following information was used for the phase diagram: i), experimental data and binary tie-lines at 24°C from POPC/PSM (26) and POPC/PCer (23) and the expected ternary phase behavior from the binary phase diagrams (42,43); ii), thermodynamic principles (the phase rule, and limitations to the two-phase/one-phase boundaries imposed by the Gibbs energy minimum principle (42)); and iii), all the experimental data obtained for these mixtures (for all the compositions scanned: number, type and compositions of the phases present and the lever rule applied to these data).

The ternary phase diagram presents seven distinct regions (Fig. 6 *A*): i), a POPC-rich fluid phase (F_1); ii), a POPC-rich fluid/PCer-rich gel phase coexistence ($F_1 + G_1$); iii), a POPC-rich fluid/PSM-rich gel phase coexistence ($F_1 + G_2$); iv), PCer-rich and v), PSM-rich gel phase (G_1 and G_2, respectively) regions; vi), a PSM-rich gel/PCer-rich gel phase coexistence ($G_1 + G_2$); and vii), a POPC-rich fluid/PCer-rich gel/PSM-rich gel phase coexistence ($F_1 + G_1 + G_2$) region.

For the sake of clarity these abbreviations will be used when referring to the different regions of the diagram. The main features of the diagram are: i), a broad POPC-rich fluid/PCer-rich gel coexistence region ($F_1 + G_1$) that extends almost to the right side of the diagram (toward PSM/PCer binary mixtures), ii), a small PSM-rich/PCer-rich gel/gel coexistence region ($G_1 + G_2$), and iii), the presence of the tie-triangle, which defines a three-phase coexistence region where the composition of each phase is given by the position of each corner of the triangle and the lever rule is valid (for further details see Appendix II).

The POPC-rich fluid region (F_1) is a small region with low PSM and PCer amounts defined by boundaries B_1 and B_2 (Fig. 6). B_1 is the boundary between F_1 and the $F_1 + G_1$ coexistence region. This line was determined from *t*-PnA fluorescence lifetime measurements. Fig. 5 shows that 2 mol % PCer is enough to induce gel phase in this PSM range (10–20 mol %). This result implies that the $F_1/(F_1 + G_1)$ boundary (B_1) lays very close to base of the diagram, toward the POPC/PSM binary mixture. B_2 is the boundary between F_1 and the $F_1 + G_2$ coexistence region. Due to thermodynamic restrictions and the negative curvature of B_1, the only possible direction of B_2 is the one shown, since the two boundaries must intersect at the left corner of the tie-triangle (*point E*, Fig. 6 *B*), B_1 crossing E toward the $F_1 + G_2$ region and B_2 toward the $F_1 + G_1$ region.

The $F_1 + G_1$ coexistence region was determined from the tie-lines for this region (T_1, T_2, T_3, and T_4, Fig. 6 *B*). The direction and length of the tie-lines together with points B and F defined the boundary B_6, between $F_1 + G_1$ and G_1 (PCer-rich gel) region. Each tie-line presented in Fig. 6 *B* was determined from the composition of the mixtures where $F_1 + G_1$ coexistence was identified (Tables 1 and 3). For a two-phase coexistence situation, the fraction of each phase is given by the lever rule. In the present case, the PCer-rich gel fraction is given by the ratio of the distance from the boundary B_1 to the mixture (distance between the *open dots* in B_1 and the *solid dots* in T_1, T_2, T_3, and T_4, respectively), total length of the tie-line connecting B_1 to B_6 (distance between the *open dots* in B_1 and in B_6) (Fig. 6 *B*). The length and direction of each tie-line were determined through an iterative method. The results that presented the smaller deviations between the following limitations were chosen: i), the tie-lines must start in B_1 and pass through the mixtures; ii), the ratio distance from B_1 to the mixture/total length of the tie-line must give the gel phase fraction for this particular mixture; iii), due to thermodynamic restrictions two tie-lines can never cross; and iv), the tie-lines should present a fanwise trend from one lateral boundary to the other, in this case from POPC/PCer binary to the EF side of the tie-triangle (Fig. 6 *B*). With the exception of T_3, all the tie-lines (T_1, T_2, and T_4) are in well accordance with these limitations. T_3 and T_4 are in a region where the tie-lines' direction is very close to the direction of EF, and therefore presents small variations. In this region an error of 1% on the composition of the mixtures may change the direction of the tie-line, resulting in divergences to the fanwise trend. Although T_3 present a small deviation to the fanwise trend, this tie-line is in respect to the remaining restrictions, and the slope of T_4 is higher than T_3 only in the third significant digit.

The region where a POPC-rich fluid, a PCer-rich gel, and a PSM-rich gel coexist ($F_1 + G_1 + G_2$) is defined by the tie-triangle EFG (Fig. 6 *B*). Applying an iterative methodology to the composition of the mixtures that present three-phase coexistence (Table 3), the tie-triangle was obtained (see Appendix II for examples of the application of the lever rule to the ternary mixtures): i), The left side of the tie-triangle (*EF*, Fig. 6 *B*) was based on the mixtures containing 2 and 4 mol % PCer and $X_{SL} = 0.3$, in which three phases are present, and the mixture containing 12 mol % PCer and $X_{SL} = 0.4$, in which only two phases coexist. In this way, this side of the tie-triangle must present a direction that allows for the first mixtures to be located inside the tie-triangle, whereas the latter mixture to be located outside (in the $F_1 + G_1$ coexistence region). Additionally, it has to be fanwise in relation to the binary tie-lines of the $F_1 + G_1$ region; ii), the base of the tie-triangle (*EG*, Fig. 6 *B*) is defined once again by the mixtures containing 2 and 4 mol % PCer and $X_{SL} = 0.3$ and 0.4, where three phases coexist. The decrease in the PCer-rich gel fraction for mixtures containing 4 mol % PCer and $X_{SL} > 0.4$ results in the slightly positive slope for this boundary; iii), the right side of the tie-triangle (*FG*, Fig. 6 *B*) was obtained accounting for the phase mol fraction of the three phases in each of the mixtures where it was identified (Table 3). To be in agreement with the fraction of PCer-rich gel for the high PCer content mixtures, the top of the tie-triangle (point *F*, Fig. 6 *B*) must lie within the 31 mol % POPC line. Therefore, point F and the boundary EG (base of the tie-triangle) define the direction of the boundary FG, thereby completing the tie-triangle EFG (Fig. 6 *B*).

After defining the tie-triangle, the POPC-rich fluid/PSM-rich gel phase coexistence region ($F_1 + G_2$) was defined. This region is delimited by the fluid/gel coexistence region of the POPC/PSM binary diagram (points *C* and *D*, Fig. 6 *B*) (26) and the boundaries B_2, EG and B_3. B_3 is the boundary between the $F_1 + G_2$ and the PSM-rich gel region (G_2), and in a similar way as B_2, due to thermodynamic restrictions it must present a direction that allows it to cross the right corner of the tie-triangle (point *G*, Fig. 6 *B*) toward the $G_1 + G_2$ (PCer-rich/PSM-rich gel/gel) coexistence region.

The B_4 and B_5 boundaries were determined based on the tie-triangle constructed, unpublished data, and calorimetric studies in SM/Cer binary mixtures (24), in a similar procedure as the one used in the study of giant unilamellar vesicles composed of an unsaturated phosphatidylcholine/Chol/SM (44). The boundary between G_2 and $G_1 + G_2$ coexistence, B_4, has a direction that allows it to cross-point G toward the $F_1 + G_2$ region (Fig. 6 *B*), to respect geometric constraints imposed by the presence of a three-phase region. In fact, two-phase boundaries crossing one point of the three-phase region must

present similar curvature and must extend to the opposite two-phase region where it originated, or extend both inside the three-phase region (42). B_5 is the boundary between the $G_1 + G_2$ and the G_1 region, where only a PCer-rich gel phase is present. The boundary B_6 and geometric restrictions derived from the Gibbs minimal energy principle (42) determined B_5 direction. Since B_6 crosses point F, expanding toward the three-phase region, B_5 must also cross F and consequently B_6, expanding inside the three-phase region. Experimental determinations were made on the right side of the ternary diagram. However, due to the technical difficulties already discussed, B_4 and B_5 are still under definition, and for that reason they are presented in Fig. 6 as dashed lines. The remainder of the phase diagram, which contains the physiological proportions of the components, is well defined and is not affected by these boundaries.

From the tie-triangle it is possible to: i), retrieve the composition of each of the three phases in coexistence, in particular the composition of the PCer-rich gel phase (point *F*), which is 31% POPC, 44% PSM, and 25% PCer (~1.8 PSM and ~1.2 POPC molecules/PCer molecule); ii), the composition of the mixtures that could not be accurately determined from the fluorescence parameters of the probes; and iii), it helps to understand in which situations PCer-rich gel forms. The PSM/PCer molar ratio for this gel phase is similar to the one obtained in POPC/Chol/PSM mixtures containing low PCer amounts (15). Additionally, the POPC/PSM/PCer ternary phase diagram offers a rational explanation for PCer-gel formation enhancement by physiological amounts of SM (~20–30 mol %). In the diagram, horizontal lines give the mol fraction of PCer. For the POPC-rich/PCer-rich fluid/gel coexistence region ($F_1 + G_1$), the tie-lines become shorter with the increase of PSM content, until it reaches the left side of the tie-triangle (EF). Hence, in this region, for the same PCer mol fraction (*horizontal line*), PCer-rich gel phase fraction is higher for 20–22 mol % PSM, as given by the lever rule. For instance, for 12 mol % PCer, PCer-rich gel fraction is higher in mixtures containing 18 mol % PSM (~25%) than in mixtures with 8 mol % PSM (~15%) (Tables 1 and 3). Another factor responsible for this effect is the POPC content of the PCer-rich gel phase at 24°C. Whereas in POPC/PCer mixtures this gel phase contains just 15% POPC (Fig. 6 *B*, point *B*), in POPC/PSM/PCer ternary mixtures the fraction of this unsaturated lipid increases up to two times (31%). Thus, the SM/Cer interaction increases POPC solubility in the Cer-rich gel, at the same time maintaining its rigidity, reflecting the synergy between SM and Cer to induce the formation of a highly ordered gel phase.

A study in POPC/PSM/PCer mixtures, has shown that PCer is able to induce the formation of PCer enriched microdomains and it was qualitatively observed an enhancement of these microdomains by PSM (19). The POPC/PSM/PCer phase diagram determined is in well accordance with this result, since the $F_1 + G_1$ region (Fig. 6 *A*), which is defined by B_1, B_6, and EF (Fig. 6 *B*) accounts for this effect. As previously explained, increasing X_{PSM}, the distance separating B_1 from B_6 decreases, and consequently the length of the tie-lines for this coexistence region also decreases. As a result, in this range of X_{PSM}, lower X_{PCer} is necessary to induce the same X_g formed by PCer at lower X_{PSM} (closer to the POPC/PCer binary phase diagram). Studies in model membranes composed of an unsaturated PC/Chol/SM/Cer have shown that low amounts of Cer (<8 mol % total lipid) are able to form Cer-rich gel domains for physiological levels of SM (14–16). Thus, the POPC/PSM/PCer diagram agrees well with these results. So, it seems feasible to conjecture that the SM fraction in many mammalian plasma membranes can be tuned to maximize Cer-rich gel formation, which would lead to a stronger response to stress stimuli.

The ternary phase diagram was determined at 24°C. At this temperature the system is well away from the T_m of any component, and the photophysical parameters of the probes in each phase are more distinct, therefore allowing for an accurate determination of the phase diagram. Additionally, a more precise $K_p^{g/f}$ of *t*-PnA for the POPC/PSM system can be obtained at this temperature, given that a broader gel/fluid coexistence region occurs at 24°C than at 37°C for these binary mixtures (26). The number, type of phase, and principal lipid in each phase are the same at 24 and 37°C and an expected general behavior of the ternary system at 37°C can be obtained from the ternary phase diagram at 24°C.

The procedures employed in this study are quite straightforward, and provide a thorough phase characterization of the system. The quantitative methodology developed can, in principle, be applied to more complex systems, by increasing the number of probes with well-characterized lipid phase-related properties, i.e., a multiprobe approach (15,23). The POPC/PSM/PCer phase diagram obtained agrees well with previous studies in similar lipid systems and explains all the experimental results obtained here. It provides a quantitative description of the ternary system studied, allowing for a better understanding of the relation between Cer biophysical and biological effects, e.g., it can be used to relate the lipid composition of plasma membrane of different cell types with the levels of Cer necessary to activate a stress response in those cells. Additionally, the phase diagram allows for quantitative studies to be carried in this ternary system, e.g., quantitative Förster resonance energy transfer for determining the size of PCer-rich gel domains, as carried out for other multicomponent lipid systems (15,33,45). The phase diagram provides also a solid base for theoretical studies, as previously done for other ternary lipid mixtures (45,46).

The plasma membrane is a dynamic entity composed of both lipids and proteins, where complex interactions between these molecules give rise to and modulate membrane domains. Therefore, the protein content of the plasma membrane should also be taken into account (47). The ternary phase diagram determined in this work provides a useful framework to rationalize how membrane domains affect the distribution of a membrane protein and vice-versa, as done, e.g., for N-Ras in raft-containing POPC/PSM/Chol membranes (48).

APPENDIX I

Determination of the fraction and composition of each phase for a three-phase situation of the POPC/PSM/PCer ternary system

The probe *t*-PnA is able to incorporate in all the three phases that can exist in the POPC/PSM/PCer ternary lipid system. Hence, the photophysical parameters for this probe were used as starting point.

From *t*-PnA mean fluorescence lifetime, the fraction of light emitted from the PCer-rich gel phase, FL_{PCer} was calculated:

$$\langle\tau\rangle = FL_{\mathrm{PCer}}\langle\tau\rangle_{\mathrm{PCer}} + FL_{\mathrm{NonPCer}}\langle\tau\rangle_{\mathrm{NonPCer}}, \qquad \text{(A1)}$$

where $\langle\tau\rangle$ is the mean fluorescence lifetime obtained for these mixtures, $\langle\tau\rangle_{\mathrm{PCer}}$ is the probe mean fluorescence lifetime in a PCer-rich gel phase, $FL_{\mathrm{NonPCer}} = (1 - FL_{\mathrm{PCer}})$ is the fraction of light emitted from the whole of the PCer-poor phases, and $\langle\tau\rangle_{\mathrm{NonPCer}}$ is the probe mean fluorescence lifetime in PCer-poor phases. For this ternary system, the probe's mean fluorescence lifetime in the PCer-poor phases is the value obtained in the absence of PCer (Fig. 4), and is given by $\langle\tau\rangle_{\mathrm{NonPCer}}$:

$$\langle\tau\rangle_{\mathrm{NonPCer}} = FL'_{\mathrm{PSM}}\langle\tau\rangle_{\mathrm{PSM}} + FL'_{\mathrm{POPC}}\langle\tau\rangle_{\mathrm{POPC}}, \qquad \text{(A2)}$$

where FL'_{i} and $\langle\tau\rangle_{\mathrm{i}}$ are the fraction of light emitted and the probe's mean fluorescence lifetime, respectively, in a PSM-rich gel (i = PSM) and POPC-rich fluid (i = POPC) phase. Note that the fraction of light emitted from each phase in the absence of PCer is not the same as in POPC/PSM/PCer mixtures, because in this latter case the fraction is calculated for the PCer-poor phases only. In the absence of PCer, the fraction of light emitted from the PSM-rich and POPC-rich ($1 - FL'_{\mathrm{PSM}}$) phases is given by Eq. A2. Knowing the total fraction of light emitted from the PCer-poor phases, the true fraction of light emitted from the PSM-rich and POPC-rich phases in ternary POPC/PSM/PCer mixtures, FL_{i}, is obtained by:

$$FL_{\mathrm{i}} = FL'_{\mathrm{i}}(1 - FL_{\mathrm{Cer}}), \qquad \text{(A3)}$$

where i = PSM or POPC.

The partition coefficient between two phases, a and b, $K_{\mathrm{p}}^{\mathrm{a/b}}$ is given by:

$$K_{\mathrm{p}}^{\mathrm{a/b}} = \frac{x_{\mathrm{a}}/X_{\mathrm{a}}}{x_{\mathrm{b}}/X_{\mathrm{b}}}, \qquad \text{(A4)}$$

where x_{i} is the fraction of probe in phase $i = a$ or b, and X_{i} is the total fraction of phase $i = a$ or b, respectively.

The ratio of emitted light fractions from two phases, a and b, is given by:

$$\frac{FL_{\mathrm{a}}}{FL_{\mathrm{b}}} = \frac{x_{\mathrm{a}}\,\overline{\tau_{\mathrm{a}}}}{x_{\mathrm{b}}\,\overline{\tau_{\mathrm{b}}}}, \qquad \text{(A5)}$$

assuming equal molar absorption coefficients in both phases, where FL_{i} is the fraction of emitted light from the phase i, x_{i}, is the fraction of probe in phase i, and, $\overline{\tau_{\mathrm{i}}}$ is the probe lifetime-weighted quantum-yield in phase i ($i = a$ or b).

Solving Eq. A4 for the ratio of the probe fraction in each phase ($x_{\mathrm{a}}/x_{\mathrm{b}}$), and replacing in Eq. A5, the following equation is obtained:

$$\frac{FL_{\mathrm{a}}}{FL_{\mathrm{b}}} = K_{\mathrm{p}}^{\mathrm{a/b}}\frac{X_{\mathrm{a}}}{X_{\mathrm{b}}}\frac{\overline{\tau_{\mathrm{a}}}}{\overline{\tau_{\mathrm{b}}}}. \qquad \text{(A6)}$$

The mol fraction ratio of each phase, a and b, ($X_{\mathrm{a}}/X_{\mathrm{b}}$) is calculated from Eq. A6.

From the previous equation the $X_{\mathrm{PCer}}/X_{\mathrm{POPC}}$ ratio is calculated. For mixtures containing 2 and 4 mol % PCer, the $X_{\mathrm{PSM}}/X_{\mathrm{POPC}}$ ratio was obtained from the POPC/PSM binary phase diagram (26). For mixtures containing those PCer amounts, DPH anisotropy values are identical to the values obtained in the absence of PCer, showing that the $X_{\mathrm{PSM}}/X_{\mathrm{POPC}}$ ratio remains unchanged for these mixtures. For mixtures containing 8 and 12 mol % PCer the substitution of PSM by PCer causes a small, but yet noticeable decrease in the PSM/POPC phase fraction ratio, which is sensed by DPH (Fig. 3). A direct comparison of DPH anisotropy values in these mixtures with the respective values obtained in the absence of PCer, allowed determining the effective PSM-rich gel phase mol fraction in respect to POPC-rich fluid phase (i.e., without interference of PCer-rich phase).

Knowing the $X_{\mathrm{PSM}}/X_{\mathrm{POPC}}$ and $X_{\mathrm{PCer}}/X_{\mathrm{POPC}}$ for the mixtures under study, the POPC-rich phase fraction is obtained, because $X_{\mathrm{PSM}} + X_{\mathrm{PCer}} + X_{\mathrm{POPC}} = 1$. The PSM-rich and PCer-rich phase fractions are determined by multiplying $X_{\mathrm{PSM}}/X_{\mathrm{POPC}}$ and $X_{\mathrm{PCer}}/X_{\mathrm{POPC}}$ by X_{POPC}.

APPENDIX II

Determination of the phase fractions within the tie-triangle of the POPC/PSM/PCer phase diagram

As previously mentioned the tie-triangle defines a three-phase coexistence region where the lever rule is valid. Here, the application of the lever rule is illustrated for the points H and I (Fig. 6 *B*). For determining the composition of each phase the planar lever EFG (tie-triangle) can be resolved into two linear levers, by drawing a straight line from any corner of the tie-triangle through point H or I to its intersection with the opposite side. For the case of point H, the top corner of the tie-triangle (F) was chosen, and the linear levers FHJ and EJG were obtained (Fig. 6 *B*). The fraction of G_1 (represented in the tie-triangle by the letter F) in the mixture H is given by:

$$\%F = \frac{JH}{JF} \times 100, \qquad \text{(A7)}$$

and

$$\%J = \frac{HF}{JF} \times 100. \qquad \text{(A8)}$$

The composition J represents the mixture of E (representing F_1 in the tie-triangle) and G (representing G_2 in the tie-triangle), so that

$$\%E = \frac{JG}{EG}\frac{HF}{JF} \times 100, \qquad \text{(A9)}$$

and

$$\%G = \frac{EJ}{EG}\frac{HF}{JF} \times 100. \qquad \text{(A10)}$$

Hence, the mixture H is composed of 46% F_1, 27% G_2, and 27% G_1. Analogously, the mixture I is composed of 84.5% F_1, 3.5% G_2, and 12% G_1.

This work (POCTI/QUI/57123/2004) and research grants (BPD/17842/2004 to R.F.M. de A., BPD/30289/2006 to L.C.S., and BPD/11488/2002 to A.F.) were supported by Programa Operacional ''Ciência Tecnologia e Investigação'' and Programa de Investimentos e Despesas de Desenvolvimento da Administração Central, Fundação para a Ciência e Tecnologia, Portugal.

REFERENCES

1. Simons, K., and E. Ikonen. 1997. Functional rafts in cell membranes. *Nature*. 387:569–572.
2. Futerman, A. H., and Y. A. Hannun. 2004. The complex life of simple sphingolipids. *EMBO Rep.* 5:777–782.
3. Simons, K., and D. Toomre. 2000. Lipid rafts and signal transduction. *Nat. Rev. Mol. Cell Biol.* 1:31–39.

4. Anderson, R. G. W., and K. Jacobson. 2002. Cell biology: a role for lipid shells in targeting proteins to caveolae, rafts, and other lipid domains. *Science*. 296:1821–1825.
5. Kusumi, A., C. Nakada, K. Ritchie, K. Murase, K. Suzuki, H. Murakoshi, R. S. Kasai, J. Kondo, and T. Fujiwara. 2005. Paradigm shift of the plasma membrane concept from the two-dimensional continuum fluid to the partitioned fluid: high-speed single-molecule tracking of membrane molecules. *Annu. Rev. Biophys. Biomol. Struct.* 34:351–358.
6. Goñi, F. M., and A. Alonso. 2006. Biophysics of sphingolipids. I. Membrane properties of sphingosine, ceramides and other simple sphingolipids. *Biochim. Biophys. Acta*. 1758:1902–1921.
7. Zheng, W., J. Kollmeyer, H. Symolon, A. Momin, E. Munter, E. Wang, S. Kelly, J. C. Allegood, Y. Liu, Q. Peng, H. Ramaraju, M. C. Sullards, et al. 2006. Ceramides and other bioactive sphingolipid backbones in health and disease: lipidomic analysis, metabolism and roles in membrane structure, dynamics, signaling and autophagy. *Biochim. Biophys. Acta*. 1758:1864–1884.
8. Cremesti, A. E., F. M. Goñi, and R. Kolesnick. 2002. Role of sphingomyelinase and ceramide in modulating rafts: do biophysical properties determine biologic outcome? *FEBS Lett*. 531:47–53.
9. Kolesnick, R. N., F. M. Goñi, and A. Alonso. 2000. Compartmentalization of ceramide signaling: physical foundations and biological effects. *J. Cell. Physiol*. 184:285–300.
10. Posse de Chaves, E. I. 2006. Sphingolipids in apoptosis, survival and regeneration in the nervous system. *Biochim. Biophys. Acta*. 1758:1995–2015.
11. Van Blitterswijk, W. J., A. H. Van Der Luit, R. J. Veldman, M. Verheij, and J. Borst. 2003. Ceramide: second messenger or modulator of membrane structure and dynamics? *Biochem. J*. 369:199–211.
12. Hannun, Y. A. 1996. Functions of ceramide in coordinating cellular responses to stress. *Science*. 274:1855–1859.
13. Bollinger, C. R., V. Teichgraber, and E. Gulbins. 2005. Ceramide-enriched membrane domains. *Biochim. Biophys. Acta*. 1746:284–294.
14. Chiantia, S., N. Kahya, J. Ries, and P. Schwille. 2006. Effects of ceramide on liquid-ordered domains investigated by simultaneous AFM and FCS. *Biophys. J*. 90:4500–4508.
15. Silva, L. C., R. F. M. De Almeida, B. M. Castro, A. Fedorov, and M. Prieto. 2007. Ceramide-domain formation and collapse in lipid rafts: membrane reorganization by an apoptotic lipid. *Biophys. J*. 92:502–516.
16. Johnston, I., and L. J. Johnston. 2006. Ceramide promotes restructuring of model raft membranes. *Langmuir*. 22:11284–11289.
17. Lopez-Montero, I., M. Velez, and P. F. Devaux. 2007. Surface tension induced by sphingomyelin to ceramide conversion in lipid membranes. *Biochim. Biophys. Acta*. 1768:553–561.
18. Holopainen, J. M., J. Y. A. Lehtonen, and P. K. J. Kinnunen. 1997. Lipid microdomains in dimyristoylphosphatidylcholine: ceramide liposomes. *Chem. Phys. Lipids*. 88:1–13.
19. Holopainen, J. M., M. Subramanian, and P. K. J. Kinnunen. 1998. Sphingomyelinase induces lipid microdomain formation in a fluid phosphatidylcholine/sphingomyelin membrane. *Biochemistry*. 37:17562–17570.
20. Holopainen, J. M., M. I. Angelova, and P. K. J. Kinnunen. 2000. Vectorial budding of vesicles by asymmetrical enzymatic formation of ceramide in giant liposomes. *Biophys. J*. 78:830–838.
21. Hsueh, Y. W., R. Giles, N. Kitson, and J. Thewalt. 2002. The effect of ceramide on phosphatidylcholine membranes: a deuterium NMR study. *Biophys. J*. 82:3089–3095.
22. Massey, J. B. 2001. Interaction of ceramides with phosphatidylcholine, sphingomyelin and sphingomyelin/cholesterol bilayers. *Biochim. Biophys. Acta*. 1510:167–184.
23. Silva, L., R. F. M. De Almeida, A. Fedorov, A. P. A. Matos, and M. Prieto. 2006. Ceramide-platform formation and -induced biophysical changes in a fluid phospholipid membrane. *Mol. Membr. Biol*. 23:137–150.
24. Sot, J., L. A. Bagatolli, F. M. Goñi, and A. Alonso. 2006. Detergent-resistant, ceramide-enriched domains in sphingomyelin/ceramide bilayers. *Biophys. J*. 90:903–914.
25. Marsh, D. 1990. Handbook of Lipid Bilayers. CRC Press, Boca Raton, FL.
26. De Almeida, R. F. M., A. Fedorov, and M. Prieto. 2003. Sphingomyelin/phosphatidylcholine/cholesterol phase diagram: boundaries and composition of lipid rafts. *Biophys. J*. 85:2406–2416.
27. Mateo, C. R., J. C. Brochon, M. P. Lillo, and A. U. Acuna. 1993. Lipid clustering in bilayers detected by the fluorescence kinetics and anisotropy of trans-parinaric acid. *Biophys. J*. 65:2237–2247.
28. Lentz, B. R. 1988. Membrane ''fluidity'' from fluorescent anisotropy measurements. *In* Spectroscopic Membrane Probes. M. L. Loew, editor. CRC, Boca Raton, FL. 13–41.
29. Sklar, L. A., G. P. Miljanich, and E. A. Dratz. 1979. Phospholipid lateral phase-separation and the partition of cis-parinaric acid and trans-parinaric acid among aqueous, solid lipid, and fluid lipid phases. *Biochemistry*. 18:1707–1717.
30. De Almeida, R. F. M., L. M. S. Loura, A. Fedorov, and M. Prieto. 2002. Nonequilibrium phenomena in the phase separation of a two-component lipid bilayer. *Biophys. J*. 82:823–834.
31. Lakowicz, J. 2006. Principles of Fluorescence Spectroscopy. Springer, New York.
32. Birch, D. J. S., and R. E. Imhof. 1991. Time-domain fluorescence spectroscopy using time-correlated single-photon counting. *In* Topics in Fluorescence Spectroscopy. J. R. Lakowicz, editor. Plenum Press, New York. 1–95.
33. De Almeida, R. F. M., L. M. S. Loura, A. Fedorov, and M. Prieto. 2005. Lipid rafts have different sizes depending on membrane composition: a time-resolved fluorescence resonance energy transfer study. *J. Mol. Biol*. 346:1109–1120.
34. Reference deleted in proof.
35. Lentz, B. R. 1989. Membrane fluidity as detected by diphenylhexatriene probes. *Chem. Phys. Lipids*. 50:171–190.
36. van Meer, G. 1998. Lipids of the Golgi membrane. *Trends Cell Biol*. 8:29–33.
37. Megha, and E. London. 2004. Ceramide selectively displaces cholesterol from ordered lipid domains (rafts): implications for lipid raft structure and function. *J. Biol. Chem*. 279: 9997–10004.
38. Lentz, B. R., Y. Barenholz, and T. E. Thompson. 1976. Fluorescence depolarization studies of phase transitions and fluidity in phospholipid bilayers. 2. Two component phosphatidylcholine liposomes. *Biochemistry*. 15:4529–4537.
39. Yeagle, P. L. 1993. The Membranes of Cells. Academic Press, San Diego, CA.
40. Koynova, R., and M. Caffrey. 1995. Phases and phase-transitions of the sphingolipids. *Biochim. Biophys. Acta*. 1255:213–236.
41. Fidorra, M., L. Duelund, C. Leidy, A. C. Simonsen, and L. A. Bagatolli. 2006. Absence of fluid-ordered/fluid-disordered phase coexistence in ceramide/POPC mixtures containing cholesterol. *Biophys. J*. 90:4437–4451.
42. Rhines, F. N. 1956. Phase Diagrams in Metallurgy: Their Development and Application. McGraw-Hill, New York.
43. Woods, L. C. 1975. The Thermodynamics of Fluid Systems. Clarendon Press, Oxford, UK.
44. Veatch, S. L., and S. L. Keller. 2005. Miscibility phase diagrams of giant vesicles containing sphingomyelin. *Phys. Rev. Lett*. 94:148101.
45. Frazier, M. L., J. R. Wright, A. Pokorny, and P. F. F. Almeida. 2007. Investigation of domain formation in sphingomyelin/cholesterol/POPC mixtures by fluorescence resonance energy transfer and Monte Carlo simulations. *Biophys. J*. 92:2422–2433.
46. Elliott, R., I. Szleifer, and M. Schick. 2006. Phase diagram of a ternary mixture of cholesterol and saturated and unsaturated lipids calculated from a microscopic model. *Phys. Rev. Lett*. 96:098101.
47. Jacobson, K., O. G. Mouritsen, and R. G. W. Anderson. 2007. Lipid rafts: at a crossroad between cell biology and physics. *Nat. Cell Biol*. 9:7–14.
48. Nicolini, C., J. Baranski, S. Schlummer, J. Palomo, M. Lumbierres-Burgues, M. Kahms, J. Kuhlmann, S. Sanchez, E. Gratton, H. Waldmann, and R. Winter. 2006. Visualizing association of N-Ras in lipid microdomains: influence of domain structure and interfacial adsorption. *J. Am. Chem. Soc*. 128:192–201.